Revisiting the Detection of Lightning Superbolts

Michael Peterson[1], Matt W. Kirkland[2]

[1]ISR-2, Los Alamos National Laboratory, Los Alamos, New Mexico
[2]A-Division, Los Alamos National Laboratory, Los Alamos, New Mexico

Corresponding author: Michael Peterson (mpeterson@lanl.gov), B241, P.O. Box 1663 Los Alamos, NM, 87545

Key Points:

- Superbolts are identified based on peak optical power. Short-duration superbolts may be missed if defined by total energy
- Normal lightning produces superbolts worldwide, but these superbolts are relatively weak - near the 100 GW threshold
- Powerful (>350 GW) superbolts occur preferentially with +CGs in oceanic wintertime storms

LA-UR 20-24558

Abstract

This study uses Fast On-Orbit Detection of Transient Events (FORTE) satellite observations to identify superbolt-class optical lightning events and evaluate their origins. Superbolts have been defined by Turman (1977) as lightning pulses whose peak power exceeds 10^{11} W. However, it has been unclear whether superbolts resulted from particular types of high-energy lightning process or whether they were the result of measurement bias. In the latter case, any decently-bright lightning process could be recorded as a superbolt if the sensor had a particularly clear sight line to the hot channel without thick clouds diluting the optical signals.

Our 12-year analysis of FORTE superbolt detections indicates that the lower superbolt energy range (~100 GW) is dominated by normal lightning, but brighter cases up to or exceeding the terawatt scale are predominantly strong +CG strokes that originate from specific types of storms. Oceanic storm systems, particularly during the winter, and especially those located around Japan are shown to produce these intense superbolts. We suggest that both interpretations of superbolt origins are correct: that some result from favorable viewing conditions and would not be identified as such by another instrument located elsewhere, and that others are associated with a unique set of physics that may merit the “superbolt” distinction.

Plain Language Summary

In 1977, Turman identified lightning that was 100 times brighter than normal in the Vela satellite data. These pulses radiated between 100 GW and multiple terawatts of optical power at the source. This observation sparked a debate as to whether these "superbolts" were caused by a certain type of powerful lightning, or were merely the result of measurement biases. Clouds dilute the optical signals generated by lightning, and reduce the optical powers recorded by satellites. If lightning occurs at the edge of the storm, then the light can travel to the space-based sensor at full intensity. Thus, any lightning event could produce a superbolt if the satellite happened to be in a favorable position to see it, and sensors elsewhere might not classify it as a superbolt.

This study analyzes FORTE satellite data to garner a better understanding of superbolts. We find that weaker superbolts (100 GW) result from both scenarios: some come from normal lightning, while others are caused by strong +CG strokes that tend to occur in oceanic regions, in the winter, and often near the coast of Japan. The most powerful superbolts (>350 GW), however, predominantly come from strong +CGs and may still merit the "superbolt" distinction.

1 Introduction

The most energetic lightning emissions have been termed "superbolts," outshining normal lightning by a factor of 100 or greater. The first measurement of a superbolt was made by the optical payload on Los Alamos National Laboratory's Vela satellite constellation, which was designed to detect nuclear explosions from space. Turman (1977) defined superbolts as having an estimated source optical power of at least 10^{11} W.

This designation of a certain class of lightning emissions as superbolts initiated a debate in the lightning research community: Do these highly-radiant events result from some undiscovered exotic lightning process that could redefine the accepted physics of lightning (new physics)? Are they produced by a particular type of lightning event enabled by favorable conditions in the electrified cloud (unique physics)? Or, are superbolts just normal lightning in ordinary storms that happen to be observed by an on-orbit sensor with an unobstructed view of the hot lightning channel (normal lightning)?

If these events represented a new or unique set of physics, then the "superbolt" designation may be appropriate. If superbolts are simply the result of measurement bias from particularly favorable viewing conditions (rather than lightning physics), then it is not warranted. Over the past four decades, evidence has accumulated that supports both possibilities.

1.1 Superbolts as a unique type of lightning

The case for superbolts representing a unique set of physics is built on similarities between Turman's superbolt Vela waveforms and ground-based optical measurements of positive-polarity cloud-to-ground (CG) strokes taken by Berger and Vogelsanger (1969), as well as a geographic and seasonal preference for superbolt activity over Japan and the northern Pacific Ocean during the winter months. This wintertime oceanic preference for superbolts differs from the behavior of normal lightning that primarily occurs over land during the warm season (Cecil et al., 2014) and usually produces negative-polarity CG strokes (Rakov, 2003).

While land-based storms produce frequent lightning and neutralize charge imbalances with each flash, oceanic storms have low flash rates and thus continue to build charge separation over long periods of time. Above-cloud aircraft electric field measurements have shown that oceanic thunderstorms generate steady-state conduction currents (Wilson currents) that are 1.7x stronger than their land-based counterparts (Mach et al., 2010) despite producing less lightning. This discrepancy in the Direct Current (DC) supplied by land and ocean storms to the Global Electric Circuit (GEC) helps to explain why the diurnal cycle of lightning disagrees with the daily change in the fair-weather electric field (the Carnegie curve) (Mach et al., 2011). Thunderstorm dynamics and the resulting precipitation structure of electrified weather differs between land and ocean. Accounting for these structural differences using space-based radar and passive microwave observations leads to the most precise reconstruction of the Carnegie curve from supply-side GEC measurements to date (Peterson et al., 2017a). This approach additionally confirms the aircraft-based finding that Wilson currents from oceanic thunderstorms are 1.7x greater than land-based storms (Peterson et al., 2018).

With oceanic storms accumulating large amounts of charge before initiating lightning, it is not surprising that oceanic flashes can be particularly powerful when they do occur. Peterson and Liu (2013) used optical Lightning Imaging Sensor (LIS: Christian et al., 2000) measurements to show that oceanic regions produced particularly bright optical lightning flashes that illuminated large areas of the surrounding storm, and that the strength and cloud-top extent of the optical emissions correlated with the lightning peak current reported by matched National Lightning Detection Network (NLDN: Cummins et al., 1998) CG strokes. Peterson et al. (2017b) later refined these results to demonstrate that oceanic flashes were still larger and more radiant than their land-based counterparts when they illuminated similar clouds under the same background illumination. The oceanic preference for optically bright lightning thus arises from physical differences in the flashes produced by oceanic storms, not from viewing conditions affecting the measurements.

The wintertime lightning off the coast of Japan that is tied to superbolt activity is a special case of oceanic lightning due to the influence of nearby Siberia on thunderstorm organization and structure. The Sea of Japan and the Pacific Ocean are prone to cold air outbreak events that generate notably shallow storms with cloud-top heights near 4 km, radar echoes extending up to 3 km, and freezing levels near or below the surface. Frontal systems further east over the Pacific may reach 8 km in height with a melting layer extending below 4 km (Yamamoto et al., 2006). Turman (1978) attributed the superbolts detected by Vela in the region to this specific type of weather pattern. In one case, the superbolt originated near the frontal occlusion in a thunderstorm with cloud-top heights of 5.5 km.

These vertically-compressed wintertime thunderstorms are known to produce large fractions of anomalous positive-polarity lightning flashes (Miyake et al., 1992). Positive-polarity CG lightning is fundamentally different from its -CG counterpart. For net positive charge to be transferred to the ground, the lightning channel must access a positive charge reservoir within the cloud. This often occurs in bolts from the blue (Rust et al., 1981), while the storm is dissipating (Mazur et al., 1998), or when lightning accesses an electrified stratiform region in a Mesoscale Convective System (Lang et al., 2004, 2017). In stratiform cases, the lightning channels can extend horizontally over hundreds of kilometers with their dendritic structures encompassing a charge region that is up to a hundred thousand square kilometers in area (Peterson, 2019a). Enormous amounts of charge from across vast regions can then be funneled down the vertical channels once they attach to ground. +CGs are usually comprised of a single stroke with continuing current that produces broad optical and Radio Frequency (RF) pulses that are hundreds of microseconds in duration (Rakov, 2003). +CGs are thought to generate strong secondary electric fields above the cloud that also lead to the generation of sprites (Pasko et al., 1995,1997). Sprites have been observed in the wintertime oceanic storms near Japan associated with superbolts, even when these storms are smaller than the minimum size threshold required for sprite activity in the continental United States (Hayakawa et al., 2004). Blanc et al. (2007) additionally linked superbolt activity with the production of such transient luminous events (TLEs). If superbolts primarily arise from these intense +CG strokes, then their distinction may well be justified.

1.2 Superbolts as normal lightning

The case for ordinary lightning generating superbolts is based on the fact that the cloud layer between the emissions source and the observing satellite dilutes the optical signals via scattering and absorption (Light et al., 2001a). If the lightning flash occurs under a thick layer of cloud, very little light will transmit through the cloud top to reach the satellite (Peterson, 2019b). This causes some lightning activity to be missed by optical space-based lightning imagers (Thomas et al., 2000). However, if a high-current lightning process like a stroke or K-change occurs near the edge of a cloud, the optical emissions can transmit to the satellite at full intensity. In this way, any optically bright CG or IC process could generate a superbolt if the viewing conditions happen to be particularly favorable.

One key scenario that where this might arise is when the space-based lightning imager is located off-nadir. If the elevation angle of the satellite is low enough, then the instrument may be able to see below the anvil shield and directly record the undiluted emissions from the exposed lightning channels in CG strokes. For satellites at higher elevation angles, optical emissions from sources near the sides of the storm can still reflect off of neighboring clouds to reach the satellite without transmitting through the full cloud depth. In either case, the signals recorded by the space-based lightning imager will be particularly bright and may reach the superbolt threshold. If superbolts are merely the result of viewing conditions and the geometry of the measurements rather than the underlying physics of the discharge, then the superbolt designation would not be merited. A second sensor at a different location would likely not classify the same optical pulse as a superbolt.

Turman (1977) noted this possibility and observed that only 20% of his superbolts were detected by multiple Vela satellites, which were positioned at different azimuth and elevation angles around the source. This fraction of reporting satellites was consistent with Lund's (1973) estimates for the probability that a flash would have a clear line-of-sight to a given satellite. Kirkland's (1999) study of superbolt-class detections by the photodiode detector (PDD: Kirkland et al., 2001) on the Fast On-Orbit Detection of Transient Events (FORTE) satellite added additional evidence that superbolt-class detections might not describe extraordinary lightning. Lightning pulses are broadened temporally by scattering in the cloud, yet the widths of Kirkland's superbolt pulses were considerably narrow compared to normal lightning. This suggests that the emissions took a relatively clear path to the satellite. Coincident NLDN measurements during FORTE PDD superbolts over the United States between April and September 1998 further showed that these highly-energetic optical pulses were generated by both positive- and negative-polarity CGs whose peak currents were as low as 10 kA. Superbolt cases were ubiquitous across the lightning-producing regions of the world (i.e., not concentrated in an anomalous region or season) including the tropical lightning hotspots (Albrecht et al., 2016). Finally, the FORTE very high frequency (VHF) waveforms that accompanied the optical superbolt detections had signatures of multiple types of CG and IC processes (Light et al., 2001b).

1.3 Anvil and stratiform superbolts

Kirkland's (1999) results do not eliminate the possibility that superbolts originate from a unique type of lightning, but they show that unique flashes and thunderstorms do not hold a monopoly on extremely bright optical pulses. Peterson et al. (2019) also demonstrated this by quantifying superbolt frequency in LIS measurements from the Tropical Rainfall Measuring Mission (TRMM: Kummerow et al., 1998) satellite according to the Precipitation Radar (PR) reported cloud type in the region illuminated by the flash. The most energetic optical pulses recorded by LIS typically occurred in one of two scenarios: "anvil superbolts" where most of the illuminated pixels were located near cloud boundaries outside of the raining area of the storm, and "stratiform superbolts" that almost exclusively illuminated raining stratiform clouds. The TRMM data implied that both interpretations of superbolt origins are correct. There exists a class of superbolts where favorable viewing conditions allow normal lightning to be particularly radiant. However, there is also a class of superbolts associated with a particular type of lightning (strong peak current +CGs) that results from a unique set of physics. Unfortunately, LIS is an integrating instrument that lacks the necessary time resolution to resolve superbolts based on peak optical power, and this made drawing parallels with Turman's (1977) sample of superbolts questionable.

The present study uses high-speed PDD detections over the complete FORTE dataset (1997-2010) to identify superbolt-class optical lightning events around the world, and coincident RF data to investigate their origins. We hypothesize that the brightest optical emissions from lightning (> 350 GW at the source) come from +CGs, while weaker superbolts (100 GW – 350 GW) result from both favorable viewing conditions and +CGs. While there is certainly a subset of superbolt-class detections that does not warrant distinction due to their dependence on how the signals are measured, we leave open the possibility that the term is justified for the +CG cases.

2 Data and Methodology

A combination of optical and RF measurements is used to examine lightning superbolts. These measurements were provided primarily by the FORTE satellite (Light et al., 2001b; Kirkland et al., 2001). NLDN measurements from across North America during the FORTE mission are also leveraged to add peak current and polarity information to the optical events recorded by FORTE. We do not show waveforms from FORTE's RF payload because the superbolts at the 10^{12} W peak optical power level either had NLDN coincidence or occurred when the RF payload was inoperable (starting in 2003). Section 2.1 describes the FORTE optical sensor package while Section 2.2 outlines our methodology for distinguishing lightning superbolts in the space-based optical measurements.

2.1 The FORTE Sensor Package

The FORTE satellite carried multiple detectors that provided a wealth of information about its recorded lightning events. FORTE's Optical Lightning System (OLS) consisted of two instruments: the Lightning Locating System (LLS), and the Photodiode Detector (PDD). These instruments recorded the steady-state background radiance of the cloud scene and then triggered on transient optical pulses caused by lightning illuminating the clouds.

The LLS was based on the LIS design with hardware provided by NASA Marshall Space Flight Center. It had a lower frame rate than LIS (a nominal 405 FPS compared to 500 FPS), and the relatively high 800-km orbit of FORTE resulted in a pixel size of 10 km projected to ground. The key difference between LLS and LIS lies in how the stream of event detections was processed. The LLS did not use LIS signal processing techniques, but instead employed a module designed by Sandia National Laboratories. Single-pixel, single integration-frame triggers known as "events" in the LIS community were not clustered into more complex lightning features representing lightning flashes during the FORTE mission.

Fortunately, the clustering algorithms that were used with LIS are well-documented in the literature (Christian et al., 2000; Mach et al., 2007). Events that describe a contiguous region on the CCD array that is illuminated by lightning during the same integration frame are clustered into "groups" in the LIS data. These group features describe the cloud region illuminated during optical lightning pulses. Groups that occur close to one another in space and time are then clustered into features representing distinct lightning flashes. We apply the LIS algorithm to the LLS event stream to construct the full lightning cluster feature data tree for the FORTE LLS record (1997–2010).

The second instrument in FORTE's optical payload was the PDD. The PDD was a high-speed (66,667 FPS) broadband (0.4–1.1 μm) photodiode detector that recorded 2–6 ms records that integrate all lightning activity across its 80° FOV. FORTE's PDD may be the closest analog to the original Vela instrumentation that reported the first superbolts. However, the FORTE PDD had two key limitations that could prevent detection in certain scenarios: (1) there was a dead time after each trigger that was approximately equal to the record length, and (2) only 20 successive triggers could be recorded over a short time. The latter caveat is the most limiting because +CGs are often preceded by extensive cloud activity that can trigger the PDD. In these cases, the PDD may exhaust its 20 records before the return stroke that would produce the superbolt.

In addition to recording lightning, the PDD was also know to trigger on energetic particle impacts and other non-lightning events that produced waveforms that are inconsistent with lightning behavior. Kirkland et al. (2001) documented a collection of filters that remove non-lightning triggers from the PDD dataset. We apply these methods to the full PDD data record used in this study to screen for artifacts.

2.2 Identifying Optical Superbolts

Superbolts have generally been identified by choosing a somewhat arbitrary energy threshold in the top 1% of lightning emissions, and then classifying anything above that threshold as a superbolt. For the FORTE PDD, we leverage the methodology used by Turman (1977) and Kirkland (1999) to identify superbolts. The optical waveforms recorded at the satellite are used to compute peak optical powers and total radiated energies at a source that is assumed to be directly below the satellite. PDD events with peak optical powers at the source that exceed 10^{11} W are classified as superbolts.

Lightning imagers (LIS, LLS) lack the high frame rates required to measure the peak optical power of the lightning pulse. Entire waveforms recorded by the PDD are captured in a single LLS frame. LIS / LLS capture photons throughout the frame duration and then report the total received radiance over this time at readout. "Superbolts" that are identified based on pulse energy measurements (Peterson et al., 2017c, Holzworth et al., 2019) may not be the same as Turman's (1977) superbolts identified based on peak optical power.

Fortunately, the FORTE PDD waveforms allow us to test whether superbolt thresholds based on energy and power describe the same flashes. Figure 1 shows two-dimensional distributions of PDD peak power against total integrated energy for the most radiant PDD events. Both parameters are normalized to estimate the emission at the source rather than the radiance received at the satellite. The thatched regions on the plot signify superbolts determined by peak optical energy (>100 GW) or total integrated energy (10^8 J). Events in the double-thatched region to the top right of the plot meet both criteria.

There were 20,348 PDD superbolt-class events across the globe based on peak optical power (>100 GW), representing the top 0.21% or all lightning detections. This fraction matches Turman's (1977) proportion of superbolts at the 100 GW level. The proportion of 3-TW events in the Vela data suggests that the FORTE PDD should have detected ~4 of these events over its mission. The PDD actually detected two such events, but one of them appears to be a Hyper-velocity Microgram Particle Impact (HMPI) at the satellite rather than a terrestrial lightning source.

Figure 1 shows how the superbolts identified based on total optical energy differ from those identified by peak optical power. For each peak optical power level (for example, 10^{10} W), there is a range of approximately 1-2 orders of magnitude in the associated total optical energy due to varying pulse widths and the limited millisecond-scale record lengths. Defining an energy threshold (say, 10^8 J) will still capture the 100-GW peak power superbolts with the broadest peaks, but the majority of the peak-power superbolts will be missed.

The brightest events in terms of total optical energy are still superbolts, but they do not represent *all* of the superbolts. Particularly quick events, -CGs for example, will be missed because they do not radiate for a long enough period to reach this total energy threshold. Thus, instruments like LIS (Peterson et al., 2017c) and GLM (Peterson, 2019a) will excel at finding +CG superbolts with their broader pulses, but may have difficulty identifying other types.

3 Results

The FORTE PDD provides similar representations of optical lightning pulses to the Vela optical system. For this reason, the high-energy events reported by FORTE will be a more appropriate analog to Turman's (1977) superbolt observations compared to superbolts identified by other types of measurement types (i.e., Holzworth et al., 2019). In the following sections, we document where and when these energetic optical pulses occur, and what types of lightning produce them.

3.1 NLDN measurements of superbolt flashes

We first examine the polarities and peak currents of the NLDN strokes that accompany superbolt-class PDD events. Kirkland's (1999) NLDN analysis of PDD events over North America between April and September 1998 showed that both +CGs and -CGs could generate >100 GW events. The NLDN data suggested that even relatively weak strokes with peak currents < 20 kA could produce superbolts. This view is not supported by Holzworth et al. (2019) whose Earth Networks Total Lightning Network (ENLTN) peak current distribution lacks superbolt cases below 100 kA.

The most likely reason for this discrepancy is the fact that the WWLLN "superbolts" identified by Holzworth et al. (2019) are measured by RF instruments rather than optically. It is thus not guaranteed (and probably unlikely) that they capture the same sample of lightning emissions as Turman (1977). Kirkland's PDD (1999) analysis supports the idea that particularly favorable sight lines can cause many types of lightning to produce superbolts, but RF measurements such as those provided by WWLLN and ENTLN are not modified by the clouds in this way. For WWLLN to record a high-energy stroke, it must be a strong CG. The fact that the ENTLN peak current threshold for matched WWLLN superbolts is identical for +CGs and -CGs further suggests that both parameters (ENLTN peak current and WWLLN energy) are highly correlated. Peak current is calculated from the Range-Normalized Signal Strength (RNSS) of a geolocated source, and is a measure of the peak E-field in the RF waveform. In this way, it is similar to the PDD peak optical power of the source calculated from the maximum in the PDD waveform. WWLLN energies, meanwhile, are calculated by integrating the E-field through the sferic, and are thus similar to the PDD total optical energy. Holzworth's (2019) comparisons between peak current and WWLLN energy are then, essentially, an RF analog to our Figure 1 for the FORTE PDD, and it is not surprising to see that RF-detected superbolts generate powerful emissions recorded by both networks.

However, the other issue that both studies share is their limited sample size of superbolt-class event coincidence with the ground networks that report peak current. Kirkland (1999) identified just 130 superbolt cases coincident with NLDN, while Holzworth et al. (2019) found just 18 matches with ENTLN. It is unclear whether either analysis is truly representative.

To generate more robust statistics, we repeat Kirkland's (1999) approach for identifying NLDN matches to PDD events and extend it to the whole FORTE record (1997 – 2010). Figure

1b shows the population density of all of these NLDN-matched PDD events. The 3.1×10^4 matched events are clustered into a relatively narrow range of total optical energies for each peak optical power than the generic PDD triggers in Figure 1. In particular, the greatest total energies per optical power seem prone to lacking NLDN coincidence. This is probably because the PDD detects the ubiquitous broad pulses from in-cloud activity (leader activity and K-changes) as well as narrow, well-defined CGs, while NLDN preferentially detected strokes during the years of the FORTE mission.

Figure 2b shows the average peak current for the PDD / NLDN matches. PDD peak optical power generally correlates with NLDN peak current, and the strokes associated with superbolts exceed 80 kA, on average. For a given peak optical power, however, the NLDN peak current tends to decrease as the total energy increases. In other words, lower peak currents are required to generate bright optical pulses (in terms of peak optical power) that have longer-duration pulses and higher total energies than quicker events. Finally, we compute the fraction of all NLDN matches that are +CGs in Figure 1c. For non-superbolt cases, the +CG fractions at a given peak-power increase from < 10% of all lightning in the lowest-energy (quickest) events to 50-100% of all lightning in the highest energy (longest-lasting) events. This supports the idea that LIS / GLM superbolts identified based on total optical energy are more likely to be +CGs than those identified by peak optical power.

Since the low sample sizes at each gridpoint in the superbolt domain of Figure 2 obscure the peak current and polarity trends, Figure 3 accumulates all PDD / NLDN matched events above certain PDD optical power levels and constructs histograms (bar plots) and Cumulative Density Functions (lines) for each level. The histograms are normalized according to the total number of PDD / NLDN matches: positive-polarity (yellow) plus negative-polarity (blue). Figure

3a shows the distributions for all PDD matches from Figure 2. These matches are most frequently 10 - 30 kA NLDN strokes (median: -21 kA, +14 kA), primarily -CGs. Figure 3b subsets the sample to only include PDD / NLDN matches where the peak optical power at the source exceeds 100 GW. The inclusion of both positive and negative strokes as well as the overall -CG dominance agrees with Kirkland's (1999) and Holzworth's (2019) findings. However, the peak currents for these 100 GW optical superbolts are notably higher than Kirkland's (1999) assessment with mean values of -73 kA and +103 kA, but still weaker than the superbolt peak current range in Holzworth et al. (2019).

If we continue increasing the PDD peak power threshold to only capture stronger events, we start to see the -CG peak erode until it is overtaken by the +CG peak. By 350 GW (Figure 3c), the histogram is dominated by +CGs that exceed 100 kA (mean: +133 kA). This change shows that the superbolts at 100 GW are generated by a different set of lightning processes than those at higher peak powers. It is thus possible that Kirkland's (1999) assessment that positive and negative CG and IC pulses may generate superbolts is correct at the 100 GW level, while terawatt-scale superbolts only occur in certain circumstances enabled by the dynamics and charge structure of the parent thunderstorm.

3.2 Global and seasonal distributions of FORTE PDD superbolts

To gauge where superbolts at different source peak power levels come from, we construct global distributions for the FORTE satellite subpoint locations during these radiant PDD events. These maps do not capture accurate source locations because the emitter could be located anywhere across PDD's FOV that is ~1200 km across. In cases where we have LLS coincidence with the PDD, we can geolocate the source to within 10 km, but many of our superbolt cases occurred while the LLS was not reporting.

Figure 4 shows the distribution of FORTE positions during PDD superbolts whose peak optical powers exceeded 100 GW at the source. As in Kirkland's (1999) analysis, these sources are distributed broadly across the globe with high concentrations of events near the tropical chimney regions in South America, central Africa, and the Maritime Continent in Asia. Weaker local maxima can also be noted leeward of the major continents, and in the Mediterranean Sea. Many of these regions were identified by Holzworth et al. (2019) as hotspots for WWLLN superbolt activity, though clear maxima over the Andes and in the North Sea are not evident in the optical PDD data.

As with the NLDN peak current histograms in Figure 3, increasing the peak power threshold changes the global distribution of superbolt cases. Figure 5 maps the global distribution of all cases whose peak powers at the source exceeds 350 GW (as in Figure 3c). The maxima near the tropical chimneys disappear entirely, leaving a few scattered (primarily oceanic) cases across the tropics. The previously-secondary peaks along the Gulf Stream, in the Mediterranean, and surrounding Japan become the most prominent features in the distribution – with the Sea of Japan / North Pacific Ocean further east producing more superbolts than any other region across the globe.

The seasonal cycles for these superbolt flashes also change based on the peak optical power threshold. Figure 6 plots the frequency of superbolts ranging from 100 GW to 500 GW for each month of the year in the northern mid-latitudes (Figure 6a), the tropics (Figure 6b) and the southern mid-latitudes (Figure 6c). There are two distinct maxima in the seasonal cycle for 100 GW superbolts in the northern mid-latitudes (Figure 6a): one in July, and another in December. The tropical curves (Figure 6b) are mostly flat over the year with three peaks at lower energies (March, July, and October). The southern hemisphere curves (Figure 6c) all have a single pronounced wintertime peak. The northern hemisphere summer peak declines as we move up in power, however. It is no longer the annual maximum by 150 GW, and is indistinguishable in the 300 GW and 500 GW curves. At these higher peak optical powers, subtropical superbolts are dominated by winter lightning in both hemispheres, in agreement with the WWLLN statistics shown in Holzworth et al., (2019).

The fact that maxima in the lightning distributions flipped from the tropics to the subtropics and from summer to winter between 100 GW and 350 GW provides further support that the composition of the lightning sample is highly sensitive to the selected peak optical power threshold. The relatively weak cases at 100 GW appear to comprise a diverse sample of "normal" lightning, but the 350+GW superbolts are dominated by +CGs that are commonly associated with wintertime oceanic storms.

3.3 The most radiant superbolts observed by the FORTE PDD

Our previous analyses have stopped at 350 GW due to the limited number of cases above this peak power level. The FORTE PDD did measure superbolts that were more radiant, however. There were a total of 38 PDD events that reached the terawatt scale, and these are listed in Table 1. Because peak optical power and total integrated optical energy are correlated (i.e., Figure 1), all of these cases generated at least 10^8 J of energy with effective pulse widths ranging from 155 μs to 542 μs. Nine of the 38 events were detected exclusively by the PDD with no other FORTE sensor reporting. This was particularly commonplace after the RF payload became permanently inoperable in 2003. There were 4 events that occurred over North America and all four had NLDN coincidence. NLDN reported peak currents ranged from 94 kA to 167 kA and were all cases of positive-polarity return strokes.

The overall brightest superbolt recorded by the PDD had a peak optical power at the source of 3.14×10^{12} W, a total integrated source energy of 7.99×10^{8} J, and an effective pulse width of 255 μs. The PDD waveform for this event is shown in Figure 7. The light curve builds quickly to its initial peak, and then optical emission persists for at least 1.3 ms afterwards. The PDD record ends before the radiance reached the background value. The slowly-varying weak emission may be continuing current from the CG. There is also a second peak 0.9 ms after the return stroke. The timing suggests that it could indicate sprite activity, but without confirmation by another instrument we can only speculate.

4 Summary

We use the full FORTE PDD record (1997-2010) to identify optical superbolts and examine the types of lightning that produce them. We find that the weaker superbolts (10^{11} W) examined by Turman (1977) in the Vela data and Kirkland (1999) in the FORTE PDD data result from a variety of lightning types. Many of these are not exceptional cases of lightning, but instead normal lightning that happens to have a clear sight line to the sensor. However, brighter events - including terawatt-scale detections – are predominantly intense +CG strokes that result from the unique dynamics of oceanic storm systems, particularly during the winter, and especially surrounding the Japanese archipelago.

The frequency and intensity of FORTE PDD superbolts is found to be consistent with Turman's (1977) results from the Vela constellation, but our results are limited by the fact that FORTE was a single satellite in low Earth orbit. Terawatt-class superbolts are exceptionally rare phenomena. In 12 years of on-orbit operations, the FORTE PDD only detected one valid lightning case that exceeded Turman's (1977) 3-TW threshold. Staring coverage from a high-speed optical instrument in a geosynchronous orbit would allow these events to be readily detected. The upcoming LANL/SNL/NNSA SENSER payload will feature instrumentation similar to the FORTE sensor package in a western hemisphere geosynchronous orbital slot that should allow these exceptionally-bright cases to be detected and compared with space-based lightning imagers (GLM, LIS), long-range ground-based networks (NLDN, WWLLN, ENTLN), and regional Lightning Mapping Arrays (LMAs) across the Americas. This wealth of data that was developed / deployed after the FORTE mission will enable unprecedented examinations of the physics behind these interesting lightning events – and perhaps finally settle the debate as to whether certain flashes merit the distinction of "superbolts."

Acknowledgments

Los Alamos National Laboratory is operated by Triad National Security, LLC, under contract number 89233218CNA000001. The FORTE PDD superbolt detections presented in this study are available in Peterson (2020). The NLDN data used in this study were provided by Vaisala, Inc. (https://www.vaisala.com/es), and may be ordered from them.

References

Albrecht, R.I., S.J. Goodman, D.E. Buechler, R.J. Blakeslee, and H.J. Christian, 2016: Where Are the Lightning Hotspots on Earth?. *Bull. Amer. Meteor. Soc.*, **97**, 2051–2068, https://doi.org/10.1175/BAMS-D-14-00193.1

Berger, K., and E. Vogelsanger (1969). New results of lightning observations, *Planetary Electrodynamics*, **1**, 489.

Blanc, E., Farges, T., Brebion, D. et al. (2007). Main results of LSO (Lightning and sprite observations) on board of the international space station, *Microgravity Sci. Technol*, **19**, 80. https://doi.org/10.1007/BF02919458

Cecil, D. J., Buechler, D. E., & Blakeslee, R. J. (2014). Gridded lightning climatology from TRMM-LIS and OTD: Dataset description. *J. Atmos. Res.*, **135**, 404-414.

Christian, H. J., R. J. Blakeslee, S. J. Goodman, and D. M. Mach (Eds.), 2000: Algorithm Theoretical Basis Document (ATBD) for the Lightning Imaging Sensor (LIS), NASA/Marshall Space Flight Center, Alabama. (Available as http://eospso.gsfc.nasa.gov/atbd/listables.html, posted 1 Feb. 2000)

Cummins, K. L., M. J. Murphy, E. A. Bardo, W. L. Hiscox, R. B. Pyle, and A. E. Pifer, 1998: A combined TOA/MDF technology upgrade of the U.S. National Lightning Detection Network. *J. Geophys. Res.*, **103**, 9038-9044.

Hayakawa, M., Nakamura, T., Hobara, Y., and Williams, E. (2004), Observation of sprites over the Sea of Japan and conditions for lightning-induced sprites in winter, *J. Geophys. Res.,* **109**, A01312, doi:10.1029/2003JA009905.

Kirkland, M. W. (1999), An examination of superbolt-class lightning events observed by the FORTE satellite. Los Alamos National Laboratory Report LA-UR-99-1685.

Kirkland, M. W., Suszcynsky, D. M., Guillen, J. L. L., and Green, J. L. (2001), Optical observations of terrestrial lightning by the FORTE satellite photodiode detector, *J. Geophys. Res*., **106**(D24), 33499– 33509, doi:10.1029/2000JD000190.

Kummerow, C., Barnes, W., Kozu, T., Shiue, J., and Simpson, J. (1998). The Tropical Rainfall Measuring Mission (TRMM) sensor package. *J. Atmos. Oceanic Technol.*, **15**, 809–817.

Lang, T. J., Rutledge, S. A., and Wiens, K. C. (2004). Origins of positive cloud-to-ground lightning in the stratiform region of a mesoscale convective system. *Geophys. Res. Lett.*, **31**, doi: 10.1029/2004GL019823.

Lang, T., S. Pédeboy, W. Rison, R. Cerveny, J. Montanyà, S. Chauzy, D. MacGorman, R. Holle, E. Ávila, Y. Zhang, G. Carbin, E. Mansell, Y. Kuleshov, T. Peterson, M. Brunet, F. Driouech, and D. Krahenbuhl, 2017: WMO World Record Lightning Extremes: Longest Reported Flash Distance and Longest Reported Flash Duration. *Bull. Amer. Meteor. Soc.* **98**, 1153–1168, https://doi.org/10.1175/BAMS-D-16-0061.1

Light, T. E., D. M. Suszcynsky, M. W. Kirkland, and A. R. Jacobson, 2001a: Simulations of lightning optical waveforms as seen through clouds by satellites. *J. Geophys. Res.,* **106**, D15, 17103–17114, doi: 10.1029/2001JD900051

Light, T. E., Suszcynsky, D. M., and Jacobson, A. R. (2001b), Coincident radio frequency and optical emissions from lightning, observed with the FORTE satellite, J. Geophys. Res., 106(D22), 28223– 28231, doi:10.1029/2001JD000727.

Lund, I . A. (1973), Joint probabilities of cloud-free lines-of-sight through the atmosphere at Grand Forks, Fargo, and Minot, North Dakota, Rep. 73-0178, Air Force Cambridge Res. Lab, Bedford, Mass.

Mach, D. M., H. J. Christian, R. J. Blackeslee, D. J. Boccippio, S. J. Goodman, and W. L. Boeck, 2007: Performance assessment of the Optical Transient Detector and Lightning Imaging Sensor. *J. Geophys. Res.,* ***112***, D09210

Mach, D. M., Blakeslee, R. J., Bateman, M. G., and Bailey, J. C. (2010), Comparisons of total currents based on storm location, polarity, and flash rates derived from high-altitude aircraft overflights, *J. Geophys. Res.*, **115**, D03201, doi:10.1029/2009JD012240.

Mach, D. M., R. J. Blakeslee, and M. G. Bateman 2011: Global electric circuit implications of combined aircraft storm electric current measurements and satellite-based diurnal lightning statistics. *J. Geophys. Res.,* **116**, D05201, doi:10.1029/2010JD014462

Mazur, V., Shao, X.-M., and Krehbiel, P. R. (1998), “Spider” lightning in intracloud and positive cloud-to-ground flashes, *J. Geophys. Res.*, **103**(D16), 19811– 19822, doi:10.1029/98JD02003.

Miyake, K., T. Suzuki, and K. Shinjou, 1992: Characteristics of winter lightning current on Japan Sea coast. *IEEE Trans. Power Delivery*, **7**, 1450-1456.

Pasko, V. P., U. S. Inan, Y. N. Taranenko, and T. F. Bell (1995), Heating, ionization and upward discharges in the mesosphere due to intense quasi-electrostatic thundercloud fields, *Geophys. Res. Lett.*, **22**, 365–368

Pasko, V. P., U. S. Inan, T. F. Bell, and Y. N. Tarenenko (1997), Sprites produced by quasi-electrostatic heating and ionization in the lower ionosphere, *J. Geophys. Res.,* **102**, 4529–4561.

Peterson, M. J., and Liu, C. (2013). Characteristics of lightning flashes with exceptional illuminated areas, durations, and optical powers and surrounding storm properties in the tropics and inner subtropics, *J. Geophys. Res.*, **118**, 11,727–11,740, doi: 10.1002/jgrd.50715

Peterson, M., W. Deierling, C. Liu, D. Mach, and C. Kalb, 2017a: A TRMM/GPM retrieval of the total mean generator current for the global electric circuit. *J. Geophys. Res. Atmos.*, **122**, 10,025– 10,049, doi:10.1002/2016JD026336.

Peterson, M. J., Deierling, W., Liu, C., Mach, D., and Kalb, C. (2017b). The properties of optical lightning flashes and the clouds they illuminate. *J. Geophys. Res. Atmos*., **122**, 423–442, doi: 10.1002/2016JD025312.

Peterson, M., Deierling, W., Liu, C., Mach, D., & Kalb, C. (2018). A TRMM assessment of the composition of the generator current that supplies the Global Electric Circuit. *J. Geophys. Res.*, **123**, 8208– 8220. https://doi.org/10.1029/2018JD028844

Peterson, M. (2019a). Research Applications for the Geostationary Lightning Mapper (GLM) Operational Lightning Flash Data Product. *J. Geophys. Res. Atmos*., **124**. https://doi.org/10.1029/2019JD031054

Peterson, M. (2019b). Using Lightning Flashes to Image Thunderclouds. *J. Geophys. Res. Atmos.*, **124**. https://doi.org/10.1029/2019JD031055

Peterson, M., S. Rudlosky, and D. Zhang (2019). Changes to the Appearance of GLM Lightning Flashes According to Thunderstorm Organization and Structure. *J. Geophys. Res.*, under review.

Peterson, M., (2020), Lightning Superbolt Data, https://doi.org/10.7910/DVN/RV39JT, Harvard Dataverse, DRAFT VERSION, UNF:6:EfCsUFiynHfRVOcQbMEWgA== [fileUNF]

Rakov, V.A., 2003: A Review of Positive and Bipolar Lightning Discharges. *Bull. Amer. Meteor. Soc.,* **84**, 767–776, https://doi.org/10.1175/BAMS-84-6-767

Rust, W. D., MacGorman, D. R., and Arnold, R. T. (1981), Positive cloud-to-ground lightning flashes in severe storms*, Geophys. Res. Lett*., **8**(7), 791– 794, doi:10.1029/GL008i007p00791.

Thomas, R., P.R. Krehbiel, W. Rison, T. Hamlin, D. J. Boccippio, S. J. Goodman, and H. J. Christian, 2000: Comparison of ground-based 3-dimensional lightning mapping observations with satellite-based LIS observations in Oklahoma. *Geophys. Res. Lett.*, **27**, 12, 1,703-1,706.

Turman, B. N. (1977), Detection of lightning superbolts, *J. Geophys. Res.*, **82**(18), 2566– 2568, doi:10.1029/JC082i018p02566.

Yamamoto, M. K., Higuchi, A., and Nakamura, K. (2006), Vertical and horizontal structure of winter precipitation systems over the western Pacific around Japan using TRMM data, *J. Geophys. Res.*, **111**, D13108, doi:10.1029/2005JD006412.

Table 1. Terawatt-class lightning superbolt cases detected by the FORTE PDD between 1997 and 2010. Only one case reached the 3-TW level, like the cases listed by Turman [1977]. All four cases around CONUS had NLDN coincidence and resulted from +CG return strokes. Reported peak currents (from top-down) were +168 kA, +95 kA, +175 kA, and +161 kA, respectively.

DATE	UTC TIME	PDD LON	PDD LAT	PEAK POWER [W]	TOTAL ENERGY [J]	PULSE WIDTH [μs]	LLS OR RF MATCH?	NLDN MATCH?
07/31/99	10:10:38.73	30.5	-33.1	1.03E+12	4.71E+08	458	YES	N/A
02/05/00	18:14:16.43	-170.0	45.6	1.03E+12	3.51E+08	341	NO	N/A
01/28/03	10:07:10.34	49.4	29.6	1.03E+12	3.69E+08	359	YES	N/A
05/23/03	22:43:53.52	27.8	-28.9	1.03E+12	3.98E+08	387	NO	N/A
12/23/05	00:49:36.80	-150.3	33.7	1.03E+12	3.40E+08	331	YES	N/A
12/30/97	09:32:19.48	-74.7	29.6	1.08E+12	3.62E+08	336	YES	YES
08/14/04	06:10:02.81	-73.3	21.4	1.08E+12	2.73E+08	253	YES	N/A
07/26/07	05:05:37.88	74.0	41.1	1.08E+12	3.15E+08	292	YES	N/A
06/13/99	21:10:16.49	-128.9	-42.1	1.13E+12	2.39E+08	212	NO	N/A
10/21/07	14:13:54.31	11.8	37.1	1.13E+12	5.77E+08	512	YES	N/A
12/18/98	12:13:01.42	-138.4	-47.5	1.18E+12	4.06E+08	346	YES	N/A
02/22/99	07:03:25.27	40.2	47.5	1.18E+12	3.87E+08	329	NO	N/A
03/25/01	09:02:37.16	-68.0	37.8	1.18E+12	5.56E+08	473	YES	YES
11/28/01	21:02:43.02	170.8	45.4	1.18E+12	2.99E+08	255	YES	N/A
01/31/03	12:11:48.02	1.2	41.8	1.18E+12	5.53E+08	470	YES	N/A
09/13/05	23:57:15.65	157.8	-34.4	1.18E+12	4.07E+08	346	YES	N/A
07/09/07	23:09:15.89	36.8	-43.9	1.18E+12	2.59E+08	220	NO	N/A
01/08/08	13:03:13.36	118.1	0.0	1.18E+12	3.06E+08	261	YES	N/A
07/05/07	15:07:10.85	-48.3	-43.4	1.23E+12	5.17E+08	422	NO	N/A
04/18/01	13:33:10.66	-68.0	39.2	1.27E+12	3.91E+08	307	YES	YES
12/13/04	00:31:46.46	148.2	10.5	1.27E+12	4.59E+08	361	YES	N/A
01/28/05	12:54:30.66	18.9	46.2	1.27E+12	5.26E+08	413	YES	N/A
01/18/09	04:14:01.16	131.0	36.2	1.27E+12	3.55E+08	278	YES	N/A
05/17/02	16:13:10.15	-87.8	35.8	1.32E+12	7.18E+08	542	YES	YES
06/12/99	09:14:11.62	3.2	55.9	1.42E+12	4.68E+08	329	NO	N/A
02/06/05	09:06:45.70	39.3	34.3	1.42E+12	4.59E+08	323	YES	N/A
04/03/05	14:30:30.49	136.1	33.5	1.42E+12	5.78E+08	407	YES	N/A
01/30/00	13:21:59.83	142.0	37.8	1.47E+12	4.00E+08	272	NO	N/A
11/24/05	06:38:18.99	5.1	36.6	1.47E+12	4.92E+08	335	NO	N/A
03/16/07	19:20:31.20	-111.1	-40.2	1.62E+12	4.01E+08	248	YES	N/A
05/07/02	19:02:58.14	48.0	40.1	1.86E+12	7.76E+08	417	YES	N/A
09/20/01	16:57:23.66	151.8	-57.6	1.91E+12	5.13E+08	268	YES	N/A
12/23/05	04:12:00.30	159.0	34.5	1.91E+12	4.68E+08	245	YES	N/A
05/15/02	16:13:17.67	101.9	-42.2	1.96E+12	3.07E+08	157	YES	N/A
12/07/05	02:52:24.32	14.6	44.8	2.01E+12	3.11E+08	155	YES	N/A
12/23/05	21:31:23.58	45.3	37.8	2.01E+12	4.89E+08	243	YES	N/A
06/10/01	14:26:40.10	75.5	64.2	2.16E+12	1.02E+09	475	YES	N/A
08/16/02	15:44:32.64	-111.5	-70.1	3.14E+12	7.99E+08	255	YES	N/A

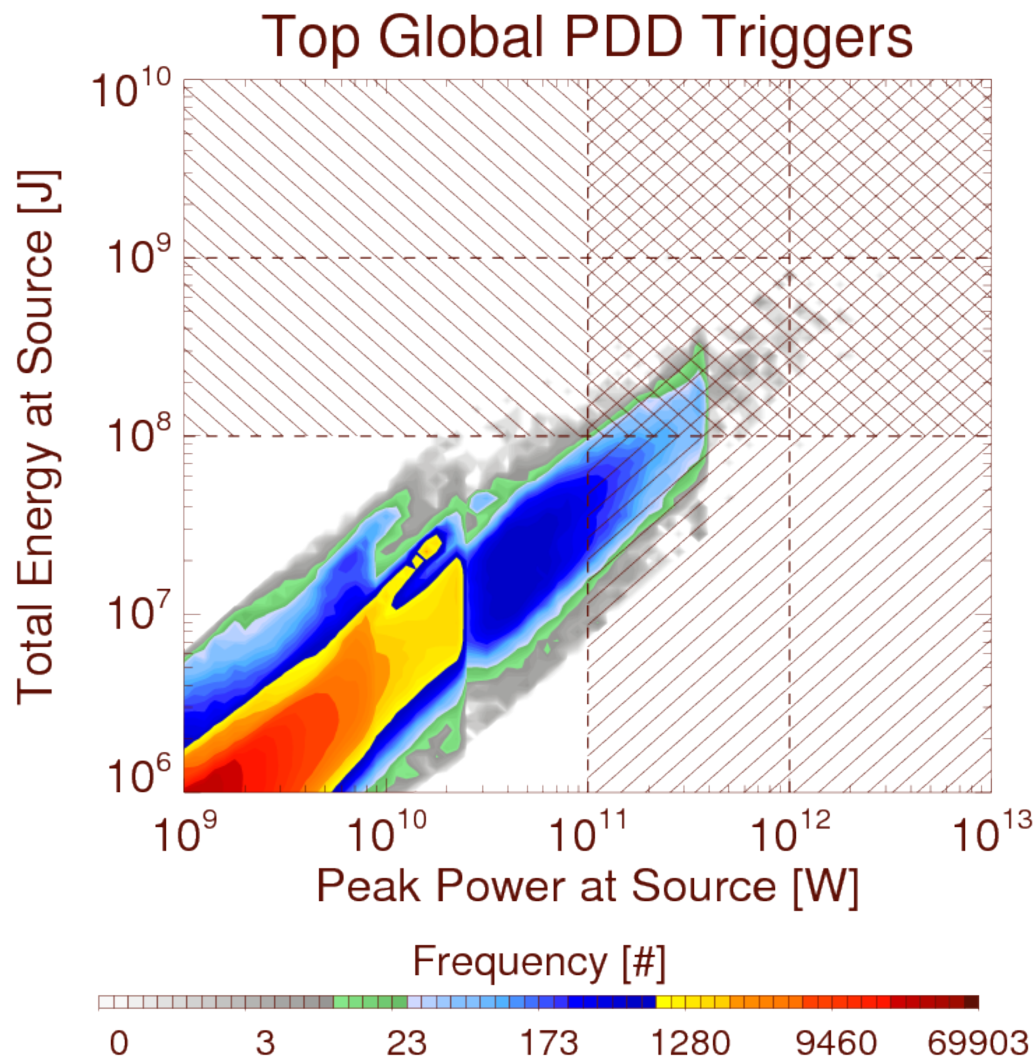

Figure 1. Two-dimensional histogram of peak optical power (abscissa) and the total integrated energy at the source (ordinate) for the brightest PDD events. Superbolts defined by peak optical power (> 100 GW) and total energy (> 10^8 J) are thatched. Only events in the double-thatched top-right region are identified as superbolts by both power and energy criteria.

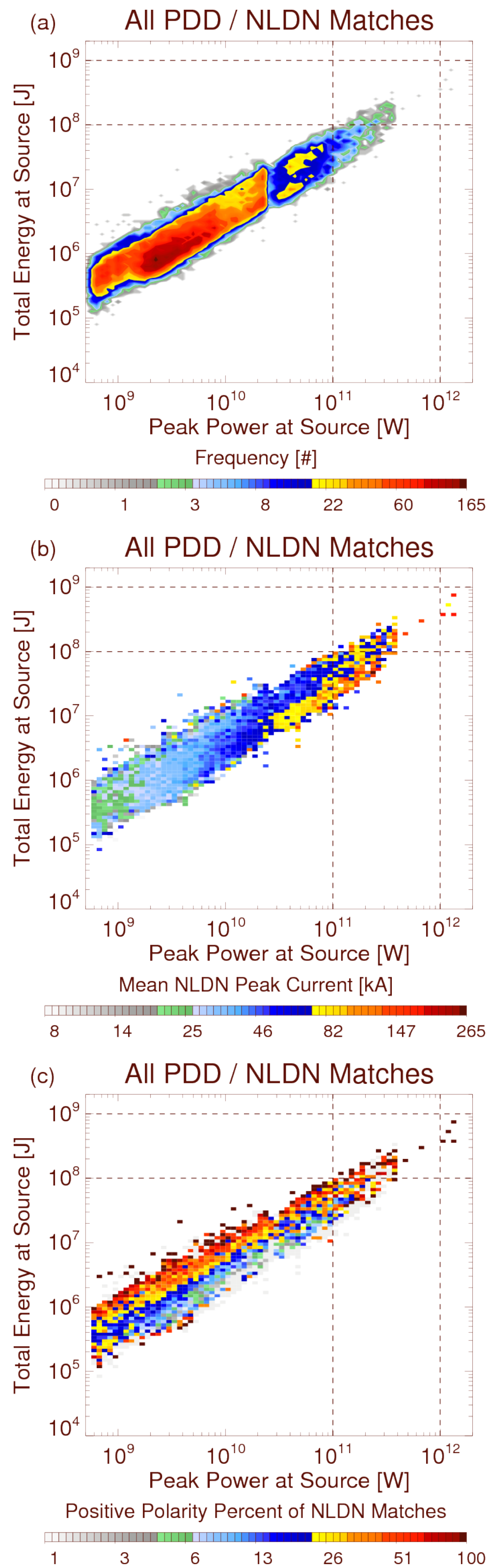

Figure 2. Two-dimensional histograms of peak optical power and the total integrated energy for PDD events with NLDN matches. Frequency (a), mean NLDN peak current (b), and the percent of NLDN matches that are positive-polarity (c) are shown.

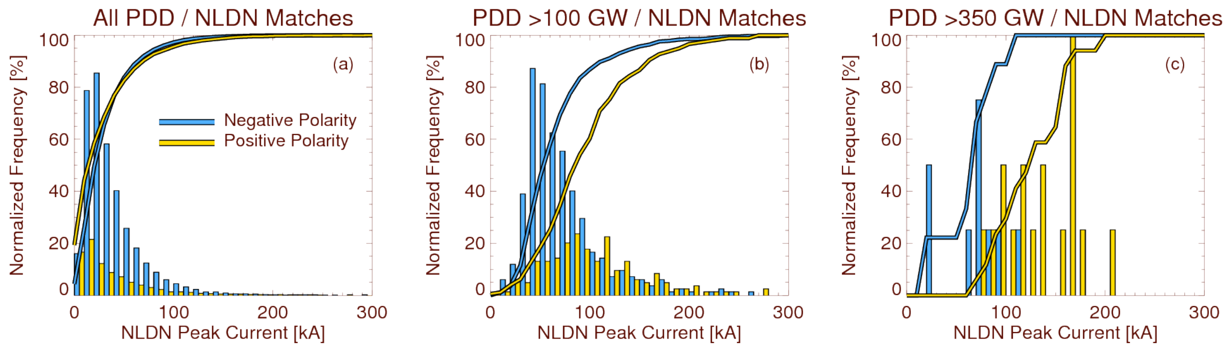

Figure 3. Histograms (bar graphs) and Cumulative Density Functions (lines) for the NLDN peak current associated with (a) all PDD / NLDN matches, (b) >100 GW PDD / NLDN matches, and (c) >350 GW PDD / NLDN matches. Most PDD matches occur with negative-polarity (blue) NLDN strokes, but high-energy superbolts (>350 GW) are disproportionately positive-polarity (yellow) NLDN strokes.

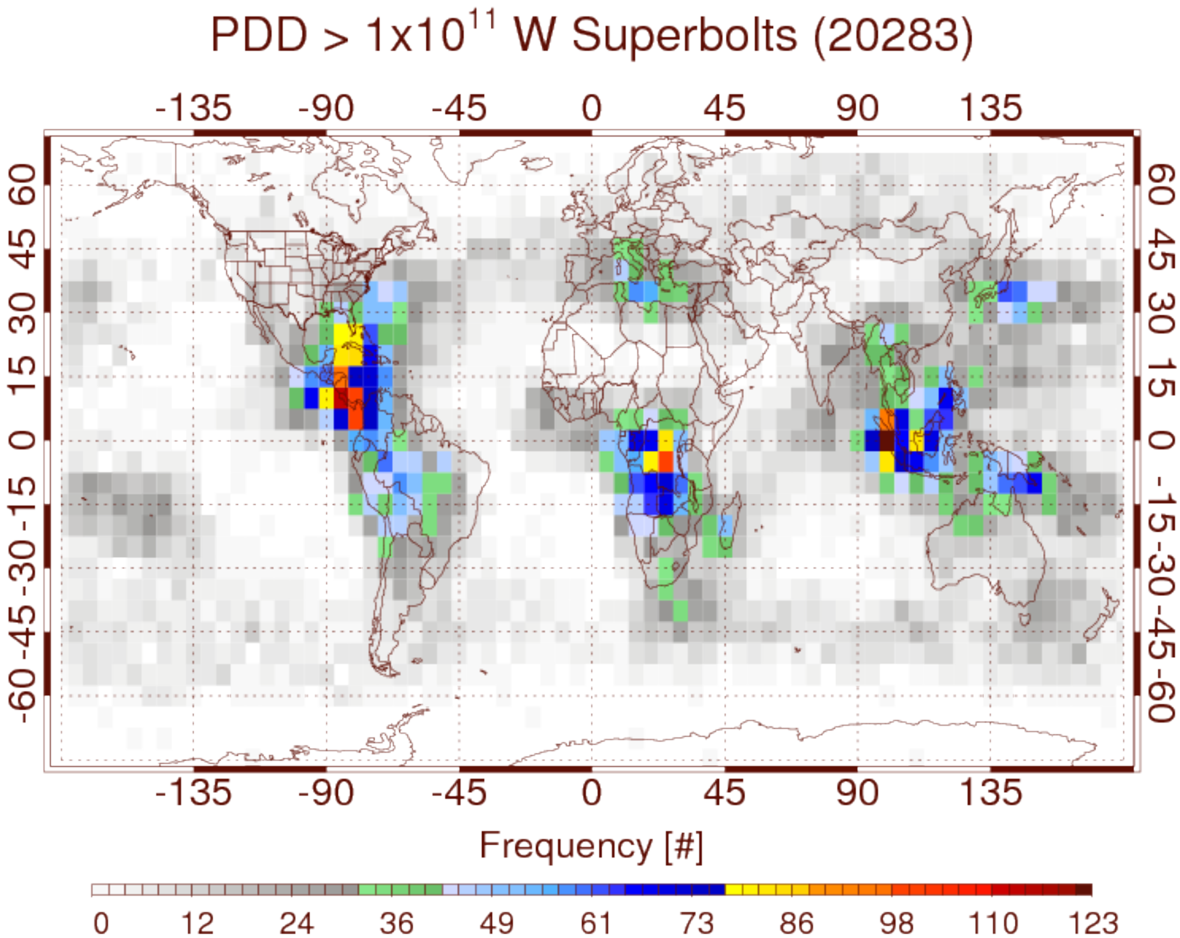

Figure 4. Global distribution of all PDD events whose peak powers at the source exceeds 100 GW. The highest concentration of superbolts are concentrated in the tropical chimney regions around Colombia / Venezuela in the Americas, the Congo Basin in Africa, and the Maritime Continent in Asia.

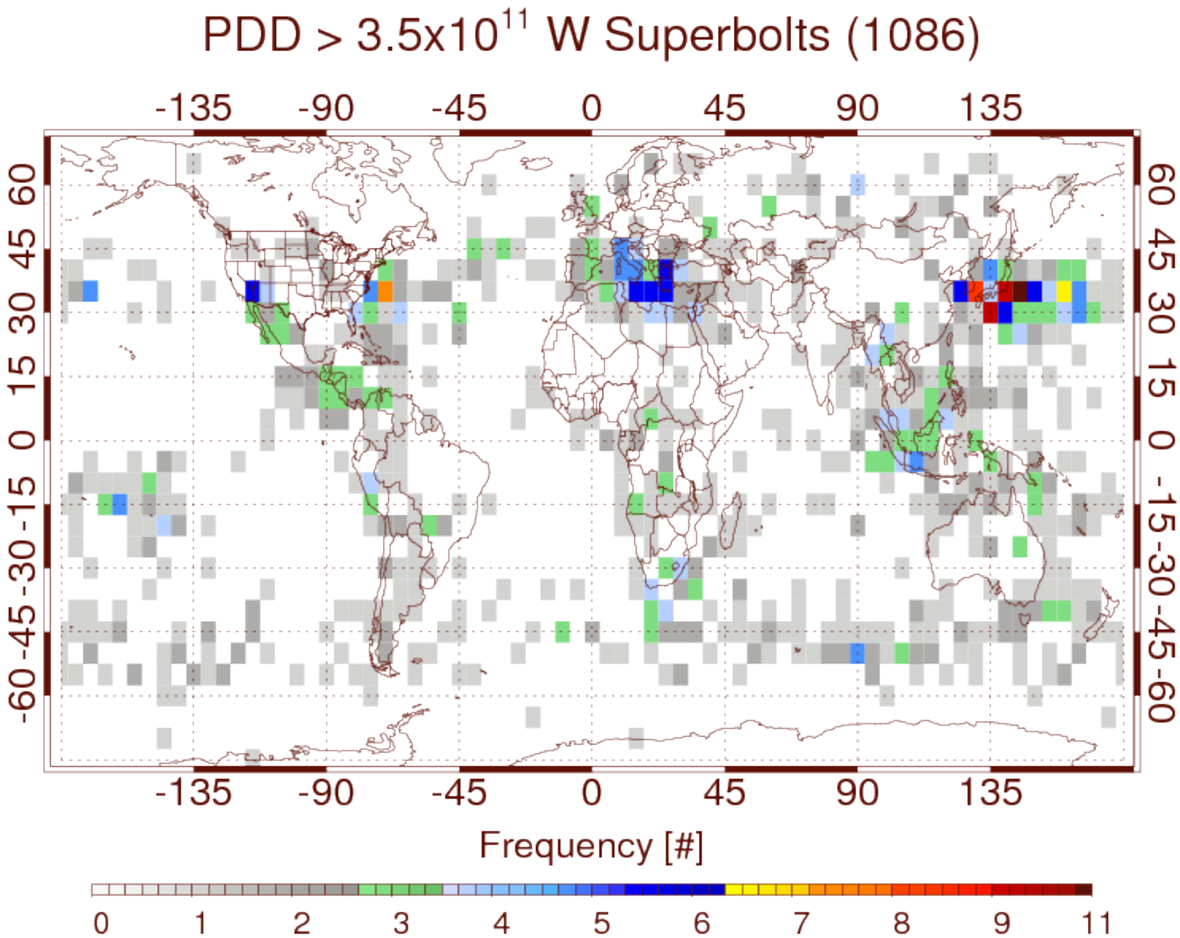

Figure 5. Global distribution of all PDD events whose peak powers at the source exceeds 350 GW. The highest concentrations of superbolt activity at this power level are found in the mid-latitudes, particularly in the Mediterranean Sea, the Sea of Japan, and the northern Pacific Ocean.

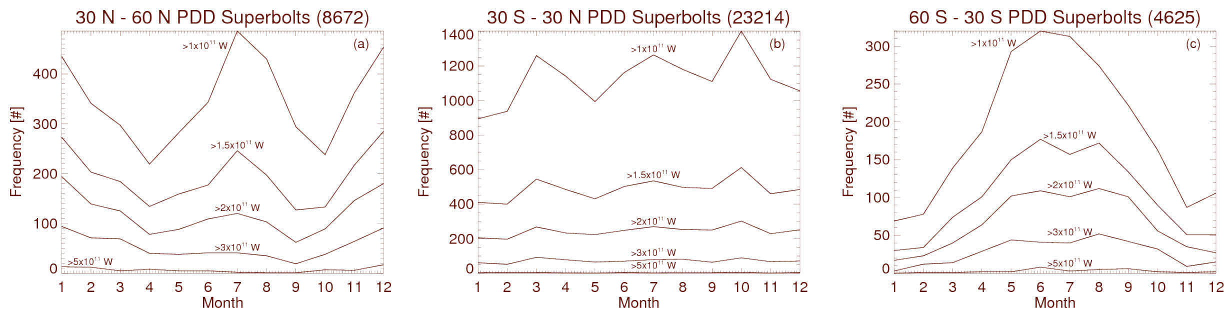

Figure 6. Annual cycles of superbolts activity over the (a) northern mid-latitudes, (b) the tropics, and (c) the southern mid-latitudes. Individual curves are drawn for various source peak power levels from 100 GW to 500 GW. Mid-latitude superbolt activity peaks in the winter months, but the northern hemisphere has a second summertime peak that erodes at higher power levels.

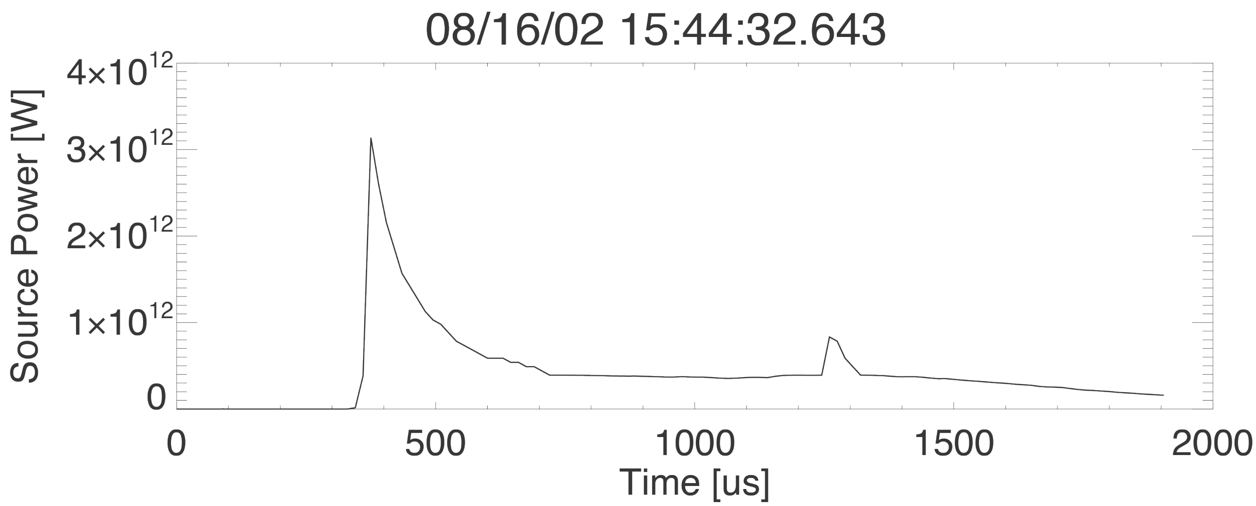

Figure 7. PDD optical waveforms from the most radiant superbolt case observed by FORTE. The intense peak was followed by 1.3 ms of continuous emission including a second weaker peak 1-ms after the first.